

# Manticore: Hardware-Accelerated RTL Simulation with Static Bulk-Synchronous Parallelism

Mahyar Emami\*  
mahyar.emami@epfl.ch  
EPFL  
Lausanne, Switzerland

Sahand Kashani\*  
sahand.kashani@epfl.ch  
EPFL  
Lausanne, Switzerland

Keisuke Kamahori†  
k-kamahori@g.ecc.u-tokyo.ac.jp  
University of Tokyo  
Tokyo, Japan

Mohammad Sepehr  
Pourghannad†  
msepourghannad@ce.sharif.edu  
Sharif University  
Tehran, Iran

Ritik Raj†  
ritik\_r@ch.iitr.ac.in  
Indian Institute of Technology  
Roorkee  
Roorkee, Iran

James R. Larus  
james.larus@epfl.ch  
EPFL  
Lausanne, Switzerland

## ABSTRACT

The demise of Moore’s Law and Dennard Scaling has revived interest in specialized computer architectures and accelerators. Verification and testing of this hardware heavily uses cycle-accurate simulation of register-transfer-level (RTL) designs. The best software RTL simulators can simulate designs at 1–1000 kHz, i.e., more than three orders of magnitude slower than hardware. Faster simulation can increase productivity by speeding design iterations and permitting more exhaustive exploration.

One possibility is to use parallelism as RTL exposes considerable fine-grain concurrency. However, state-of-the-art RTL simulators generally perform best when single-threaded since modern processors cannot effectively exploit fine-grain parallelism.

This work presents *Manticore*: a parallel computer designed to accelerate RTL simulation. *Manticore* uses a *static bulk-synchronous parallel* (BSP) execution model to eliminate runtime synchronization barriers among many simple processors. *Manticore* relies entirely on its compiler to schedule resources and communication. Because RTL code is practically free of long divergent execution paths, static scheduling is feasible. Communication and synchronization no longer incur runtime overhead, enabling efficient fine-grain parallelism. Moreover, static scheduling dramatically simplifies the physical implementation, significantly increasing the potential parallelism on a chip. Our 225-core FPGA prototype running at 475 MHz outperforms a state-of-the-art RTL simulator on an Intel Xeon processor running at  $\approx 3.3$  GHz by up to 27.9 $\times$  (geomean 5.3 $\times$ ) in nine Verilog benchmarks.

## 1 INTRODUCTION

The long-anticipated end of Moore’s Law and Dennard Scaling has dramatically increased commercial and academic interest in computational accelerators [2, 7, 14, 25, 28, 31, 33]. As with any hardware artifact, accelerators require many iterations of design, debugging, testing, and software development. Detailed hardware simulation is at the heart of this activity, and a simulation’s turnaround time and throughput can directly affect designer productivity and product quality.

Designers, however, face a dilemma. Software RTL simulators offer much faster turnaround and better visibility into the hardware than prototypes (e.g., on FPGAs). Simulation, however, runs much slower than hardware, which can be a bottleneck when simulating a large design, running a long execution, or performing extensive testing.

Since the advent of multicore, parallelism is the preferred approach to improve software performance. RTL simulation appears to offer many opportunities for parallelism. Indeed, hardware description languages (HDL) such as Verilog or VHDL [13] contain parallel constructs for describing parallel hardware components that run independently and synchronize only at clock edges. However, designers want circuits that run at high clock frequencies, which constrains the number of gates between clock edges. Therefore, a realistic RTL design comprises many *tiny*, independent computation tasks. The resulting fine-grain parallelism interacts poorly with multicore processors because frequent synchronization and communication are (relatively) costly.

This work explores a different approach to improving RTL simulation performance. We design and construct *Manticore*, an architecture for parallel RTL simulation (i.e., a simulator accelerator). *Manticore* leverages a *static bulk-synchronous parallel* (BSP [39]) execution model that virtually eliminates dynamic overheads of RTL simulation through static scheduling. Similar to computers such as MIT’s Raw machine [40], *Manticore* relies entirely on its compiler to statically schedule resources and communication. Because RTL code rarely exhibits long divergent code paths, static scheduling is feasible. The resulting scheduled communication and synchronization run without overhead, so fine-grain interactions among cores are efficient. Moreover, static scheduling dramatically simplifies the microarchitecture, significantly increasing the parallelism possible on a chip.

*Manticore*’s compiler accepts single-clock RTL designs and generates binary code that runs on a *Manticore* coprocessor. Compilation time is comparable to software compilers, offering software development-like turnaround but a significantly faster simulation rate. We prototyped *Manticore* on an FPGA, and it outperforms Verilator [35] (the fastest open-source RTL simulator) running on a Xeon processor by up to 27.9 $\times$  (geomean 5.3 $\times$ ), despite running at a

\*Both authors contributed equally to this research.

†Work done during EPFL internship.

fraction of the Xeon processor’s clock speed. Hardware-accelerated simulation offers a designer a path out of the dilemma above by optimizing “time to result.” Small experiments and tests can run on a software simulator with very fast turnaround. More extensive experiments and tests can run on Manticore, with slightly slower compile times but much faster execution. And hardware prototypes can be reserved for full-system simulation, operating system bring up, and software development.

The chief contributions of this work are:

- The application of a static BSP execution model to RTL simulation,
- The Manticore architecture that supports fine-grain parallelism in the simulation of RTL through static BSP,
- A compiler that finds parallelism in RTL code and statically schedules it to run effectively on Manticore,
- A high-performance FPGA prototype of Manticore,
- An extensive evaluation analyzing the superior performance of Manticore over state-of-the-art software RTL simulation.
- A demonstration that the fine-grain parallelism in RTL simulation can be effectively exploited.

We will open-source Manticore’s compiler and hardware upon publication.

The paper is organized as follows: §2 discusses RTL simulation and quantitatively explores the inherent limitation of general-purpose processors for exploiting its fine-grained parallelism. §3 presents the static BSP execution model. §4 presents Manticore’s architecture. §5 discusses a high-performance implementation of Manticore. §6 presents the compilation techniques used to exploit Manticore’s hardware. §7 evaluates Manticore’s performance and design decisions. §8 discusses limitations and future directions. §9 surveys closely related work. Finally, §10 concludes.

## 2 BACKGROUND

RTL simulation is performed at two granularities: *timing-accurate*, or *cycle-accurate*. Timing-accurate simulation timestamps value changes to model gate delays accurately. By contrast, cycle-accurate simulation captures value changes only at clock edges. Early in the design process, when logic delays are unknown, cycle-accurate and timing-accurate simulation are equivalent.

Cycle-accurate simulators are implemented in two ways: *event-driven*, or *full-cycle*. An event-driven simulator observes signal values and *dynamically* schedules operations, which avoids needless re-evaluation of unchanging circuit elements. By contrast, full-cycle simulators use a single compile-time schedule to ensure values are computed in the correct order.

This work focuses on full-cycle, cycle-accurate simulation. Full-cycle is generally faster than event-driven simulation despite the unnecessary work since the cost of monitoring and scheduling events can outweigh the benefit of suppressing unnecessary execution [4].

### 2.1 Verilator RTL simulator

This section describes Verilator [35], our baseline software RTL simulator. Verilator is a popular open-source, full-cycle simulator widely used by academia and industry. It is believed to be faster than

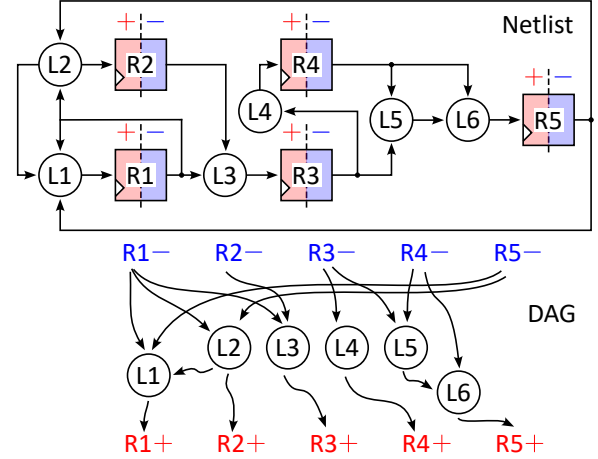


**Figure 1: An example single-clock netlist (top) and its DAG representation (bottom). Circles represent gates and rectangles represent registers.**

commercial and other open-source simulators [35]. It performs full-cycle simulation by generating a C++ simulation model. Verilator produces C++ code from an abstract syntax tree (AST) of inlined and optimized RTL code. The generated C++ is highly optimized; Verilator maximizes performance with branch prediction hints, short-circuitable branch conditions, and memory prefetches.

Hardware description languages model circuits in the form of a *netlist*. A netlist is a directed graph whose nodes are circuit cells (gates, registers, and memory banks) and whose edges are the wires connecting them. A netlist graph can be made acyclic by splitting the state nodes (e.g., registers) into a *next* and *current* value. For example, the top part of Fig. 1 contains a netlist in which circles represent gates and rectangles represent registers. The corresponding directed acyclic graph (DAG) is at the bottom where the *next* and *current* values are denoted by + and -, respectively.

Simulating RTL executes the netlist DAG while respecting precedence relations. A simulated cycle concludes when all *next* register values are computed using the *current* register values. The *current* values are then updated from the newly computed ones, and the process repeats. The DAG, moreover, fully expresses the inherent parallelism of an RTL circuit as an interpreter can simulate independent paths through the graph in parallel.

Verilator uses such a DAG to parallelize RTL simulation. To do so, Verilator partitions its DAG into *macro-tasks*, the atomic units of work that run asynchronously. It then combines these tasks into larger units appropriate for multicore parallelism. Initially, each DAG node comprises a macro-task. Verilator increases the granularity of computation by combining smaller macro-tasks that share an edge into a single task using Sarkar’s algorithm [32]. Doing so eliminates the communication of values along the edge, but can increase the critical path of the macro-task graph since the nodes in a macro-task execute sequentially. Verilator repeatedly merges the macro-task that produces the smallest increase in the critical path. It does so until it reaches a heuristic threshold for the critical path. Verilator then statically assigns macro-tasks to a pool of threads. At runtime, a macro-task can start its execution when

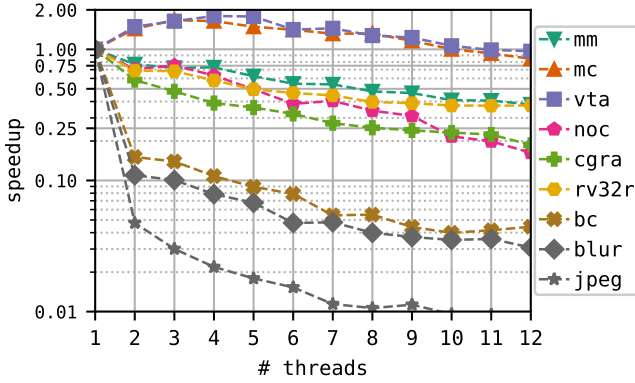


Figure 2: Verilator’s multi-threaded performance normalized to single-thread execution (log-scale).

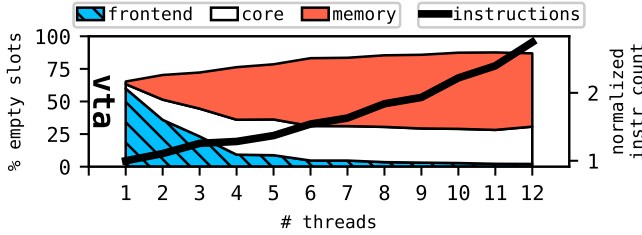


Figure 3: Verilator’s pipeline behavior (vta). Empty pipeline slots are broken down into the ones caused by I-cache misses (frontend), data hazards (core), and data memory stalls. The left vertical axis shows the percentage of empty pipeline slots. The right vertical axis shows instruction count normalized to single-thread execution.

its preceding macro-tasks finish. Atomic fetch-and-add operations (i.e., user-space spin-locks) synchronize the macro-tasks.

## 2.2 Parallel Simulation Performance

Despite its sophisticated optimization, Verilator is often unsuccessful at exploiting multicore parallelism. Fig. 2 illustrates the mismatch between RTL simulation and modern computers. It reports the parallel performance of nine RTL workloads (described in §7) on Verilator. The experiment ran on a Xeon E5-2680 v3 processor with 12 physical cores. Two of the benchmarks experience an insignificant 2× speedup, while others’ performance degrade sharply (up to 100× slowdown).

We profiled the workloads to understand this performance degradation. A few benchmarks are initially processor I-cache bound (e.g., vta in Fig. 3). These are the only ones to achieve a modest speedup with more CPU threads. By partitioning work across threads, each core executes less code, increasing instruction locality and reducing I-cache misses. However, as the number of CPU threads increases, data memory stalls rise sharply, accounting for about 70% of all empty CPU pipeline slots. Additionally, the CPU’s dynamic instruction count increases on all benchmarks by a factor of 3–100×. The increased instruction counts reflect the instructions executed by spin-loop synchronization, which grows with the number of cores

because of increased lock contention. The cost of frequent synchronization quickly overshadows the performance gains from parallel execution or improved cache locality (see Fig. 13 in the Appendix).

For the similar reasons to why full-cycle outperforms event-driven simulation, we propose to improve the performance of RTL simulation using *compile-time synchronization* to eliminate runtime overhead. Doing so requires a co-designed architecture to handle the fine-grain computation and communication. This work presents a compiler-synchronized execution model for RTL simulation and our hardware architecture that implements it.

## 3 THE STATIC BSP EXECUTION MODEL

This section proposes our *Static BSP* execution model. Static BSP is a low-overhead execution model for parallel RTL simulation. It is inspired by Valiant’s bulk-synchronous parallel (BSP) execution model [39]. Fig. 4 outlines the components of static BSP. Like the original BSP model, ours consists of a system of networked processors that alternate between phases of local computation and cross-processor communication.

### 3.1 Runtime Synchronization Freedom

The original BSP model relied on a *runtime barrier* to synchronize at the end of communication (before processors start a new computation phase). Static BSP eliminates this runtime barrier with a *compile-time schedule*. Static BSP requires hardware to expose a *deterministic* interface so that a compiler can schedule computation and communication. The compiler replaces runtime barriers with delay operations (e.g., sleep in Fig. 4) that ensure all processes start the next phase at the same time.

### 3.2 Applying Static BSP to RTL Simulation

To parallelize RTL simulation, we partition the RTL netlist DAG (the bottom of Fig. 1) into multiple independent graphs by creating a DAG per sink node. The computation in each graph consumes multiple *current* register values and produces exactly one value in a *next* register. The DAGs are independent and so can be evaluated in parallel. Once all DAGs are simulated, the computed *next* values become the input to the DAGs that consume them, and a

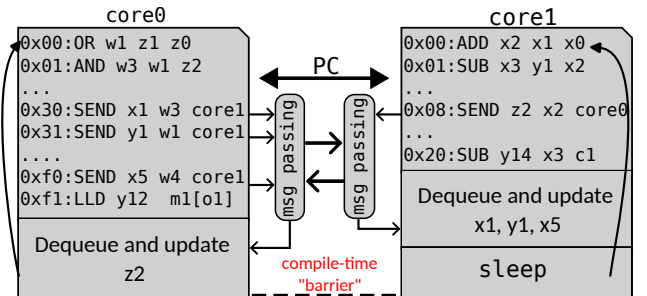


Figure 4: The static BSP execution model. Each core performs a local computation and then sends its result to the cores that need it for the next computation phase. Cores wait (with compiler-inserted NOPs) until all communication completes before starting new computation.

new simulation cycle starts. However, in practice computation and communication always overlap.

RTL simulation can be statically analyzed and scheduled because RTL code rarely has long-lived divergent code paths. This enables a conservative, yet efficient schedule of divergent code paths while maintaining determinism.

In the context of RTL simulation, we call a complete iteration of the computation *and* communication phases a *virtual cycle (Vcycle)*. We do so to distinguish between *RTL cycles (Vcycle)* and the *clock cycles* of the processor that is running the simulation.

## 4 MANTICORE ARCHITECTURE

We now describe Manticore, an architecture whose fully-deterministic runtime behavior satisfies static BSP’s requirements.

### 4.1 Key Ideas

We now list Manticore’s most salient features which permit deterministic behavior.

- Manticore consists of multiple simple cores that communicate over a statically-scheduled network-on-chip (NoC) (Fig. 5).
- Cores communicate through *message passing* since shared memory’s dynamic performance and communication make static scheduling difficult.
- A compiler controls how messages are scheduled and routed between cores to ensure deterministic delivery.
- Instructions are *statically partitioned* across cores and stored in fixed-latency on-chip memories. This eliminates frontend stalls, assuming each program partition fit a core’s instruction memory.
- Manticore replaces branches with *predication* and executes all code paths.
- Each core accesses only the program state stored in its register file and local, fixed-latency scratchpad memory. The scratchpad holds the small (few KiBs) on-chip memories typically found in RTL designs (FIFOs, etc.).
- When the program state will not fit in the scratchpads (e.g., large processor caches or memories), a *privileged core* accesses an off-chip DRAM memory using a *global stalling* mechanism to ensure all cores and the NoC remain in lock-step.

### 4.2 Instruction Set

We briefly describe unconventional aspects of the ISA specific to RTL simulation.

Each core supports 32 programmable *functions*, which accelerate chains of bitwise logic operations with up to four inputs. For example, consider the expression  $(a \& 0xf) | (b) | (c \& 0x3) | (d \wedge 0x1)$ , with  $a, b, c,$  and  $d$  being operands<sup>1</sup>. A *single* custom instruction can replace these six instructions (see §6.2). Programmable functions are loaded into a processor at boot time.

The Expect  $rs1, rs2, eid$  instruction raises an exception  $eid$  if the values of registers  $rs1$  and  $rs2$  differ. Exceptions are used to invoke services from the host processor (e.g.,  $\$display$

and  $\$stop$  in Verilog). Exceptions, like global memory accesses, stall the execution of all cores and the NoC until they are resolved. Instructions capable of globally stalling the execution are *privileged* and reserved for a single core to permit an efficient implementation (see §5.3).

Each core has a scratchpad memory (up to 128KiB) for local load and store operations. Loads execute unconditionally, but stores are predicated. Global load and store (predicated) instructions are privileged and access large, off-chip memories using 48-bit addresses. From the perspective of a compiler, both global and local memory instructions have the same predictable access latencies since the long off-chip latency is masked by stalling all cores and the NoC until an access completes.

The producer of a value initiates communication with a Send instruction, the only way cores communicate. The Send  $rt, rs, tid$  instruction invoked by a core  $sid$ , requests target core  $tid$  to update its register  $rt$  with the value of register  $rs$  from core  $sid$ . The register update is delayed<sup>2</sup> until the end of a Vcycle, as depicted in Fig. 4.

## 5 MICROARCHITECTURE

This section describes Manticore’s microarchitecture and its efficient FPGA implementation. We prototype Manticore on a Xilinx UltraScale+ FPGA (the Alveo U200 datacenter FPGA card). The ideas, however, are general and apply to other FPGAs and ASIC implementations.

Fig. 5 depicts an example 6-core Manticore grid. Manticore operates as a coprocessor for a *host* (e.g., an x86 processor), which loads programs on Manticore and handles exceptions or termination. The host communicates with the grid by reading and writing specific registers and has full access to Manticore’s DRAM.

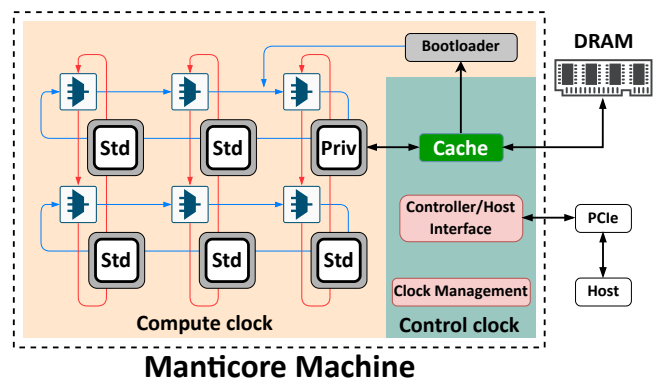


**Figure 5: A Manticore grid of processors on a uni-directional 2D torus NoC. The cores and the NoC reside in the *compute* clock domain, while all other components reside in the *control* clock domain. The privileged core is connected to a cache and can access off-chip DRAM.**

<sup>1</sup>Taken from picoRV32, a multi-cycle RISC-V processor.

<sup>2</sup>The delay is compiler-enforced (it is not architectural).

## 5.1 Pipeline Implementation

Each core is implemented with a simple 14-stage pipeline. The pipeline is simple because we remove expensive bookkeeping logic (e.g., interlocks and scoreboards) and delegate them to the compiler. The logical pipeline is the usual five stages: fetch, decode, execute, memory access, and writeback. Each stage is internally pipelined to achieve a high clock frequency. A block diagram of the pipeline is available in the Appendix (Fig. 14). RTL code contains structures of various bit widths that are typically narrower than a conventional processor’s 32-bit word size. Manticore uses a 16-bit datapath to match the native width of the FPGA’s hard DSP units. This further simplifies the hardware and enables higher clock frequencies.

Instructions are fetched over two cycles from a dedicated instruction memory mapped to a 4096×64 URAM. URAMs are large 36 KiB on-chip memories.

Deep pipelines require a large register file to avoid stalls. We use a 2048-element register file in which all registers are exposed to the compiler to avoid expensive renaming logic in hardware (similar to the Raw machine [40]). We implement the register file using BRAMs. BRAMs are configurable 4.5 KiB on-chip memories that support multiple addressing modes. We use a 2048×17 addressing mode where the lower 16 bits contain the register value, and the most-significant bit contains an *overflow bit* used by wide addition instructions. The size of the register file requires additional pipelining for reads. This makes decoding three stages long. Some instructions can read four values from the register file and write a single result. This requires four read ports and one write port, which BRAMs do not natively support<sup>3</sup>. We use four identical BRAMs that are write-mirrored to read four values simultaneously.

The execute stage consists of two computational units pipelined over four stages. The ALU handles most standard instructions using a hardened FPGA DSP. The custom function unit (CFU) is implemented as a small 32×256 memory made of LUTRAMs. LUTRAMs are FPGA primitives used to implement shallow memories. A 1-bit 4-input boolean function is canonically defined by the 16 bits of its truth table. Manticore’s datapath is 16 bits wide, so we extend this idea to a wider 16-bit truth table using  $16 \times 16 = 256$  bits of memory per function.

Scratchpads are mapped to a URAM, with two cycles to access and one cycle to reshape. We reshape a 4096×64 URAM into a 16384×16 memory by using byte-strobes on the write path and multiplexers on the read path.

## 5.2 Network-on-Chip

The cores communicate over a uni-directional torus NoC with buffer-less switching and dimension-ordered routing [17]. We chose this design to reduce routing congestion on the FPGA and to support a high clock frequency.

Switches do not queue messages and immediately route them. A switch drops the input message if the target link is busy. The compiler statically schedules Send instructions to avoid data loss. Manticore’s deterministic execution makes this possible.

Links carry 27 bits of payload, and a few<sup>4</sup> bits to specify the target core address. Arriving messages at a core are queued and

received only when the core finishes a Vcycle (see Fig. 4). We use the instruction memory and its unused write port as the queue to save resources. We do this by encoding an incoming message as an instruction and pushing it to the end of the instruction memory. The core then executes it like any other at the end of a Vcycle (see Fig. 14 in the Appendix).

## 5.3 Global Stall

In our current implementation, the privileged core is connected to a 128 KiB direct-mapped, write-allocate, write-back cache backed by a DRAM bank. The cache is implemented using 4 URAMs and has a fixed latency whether an access misses or hits. A cache miss triggers a DRAM access, which stalls all cores and the NoC until the DRAM access is complete. Therefore, from the compiler’s point of view, a global memory access appears to all cores as a fixed latency operation independent of DRAM latency.

Implementing the stall by routing a global signal from the cache to each core does not scale to hundreds of cores. Instead, we take advantage of the FPGA’s clock gating primitives to achieve this functionality. All parts of Manticore that operate in strict lockstep (the cores and the NoC) reside in the *compute* clock domain. The rest of the logic that deals with non-determinism resides in the *control* clock domain (see Fig. 5). The two domains are frequency-matched and phase-aligned. The logic in the control domain has the ability to *halt* or *resume* the compute clock with a global clock buffer. Fig. 5 highlights these two clock domains.

We took great care in implementing the clock gating logic to minimize its effect on scalability. For instance, there is no logic delay from the clock enable signal to the clock buffer that receives it. The result is that clock gating logic is nearly independent of the number of cores.

With global clock gating, computation is frozen on a cache request and resumed once it completes. The same mechanism is used to stall the compute domain when an exception occurs so that exceptions are precise. Control is then transferred to the host machine and computation resumes at the host’s command.

## 6 COMPILER

Manticore’s hardware is co-designed with its compiler, which is responsible for extracting parallelism, custom function synthesis, and instruction scheduling. Fig. 6 sketches the compilation process. The compiler operates on two related intermediate representations (IR): netlist and lower assembly. Both use static single assignment and can be interpreted in software. The lower interpreter is a full-fledged ISA simulator parameterized by the hardware configuration. We used the interpreters extensively to validate the compiler passes.

We based the Verilog frontend on Yosys [42]. We extended Yosys to support basic system calls such as \$display and \$stop that are required for simulation. After parsing the Verilog input, the frontend performs a few optimizations and emits netlist assembly. Because of the semantics of RTL code, instructions in netlist assembly are unordered and have arbitrary-width operands.

The backend orders the instructions and applies simple optimizations (dead code elimination, constant folding, and common sub-expression elimination). We then transform the netlist assembly

<sup>3</sup>BRAMs and URAMs have one read port and one write port.

<sup>4</sup>Varies based on the grid size, e.g., 8 bits for a 15×15 grid.



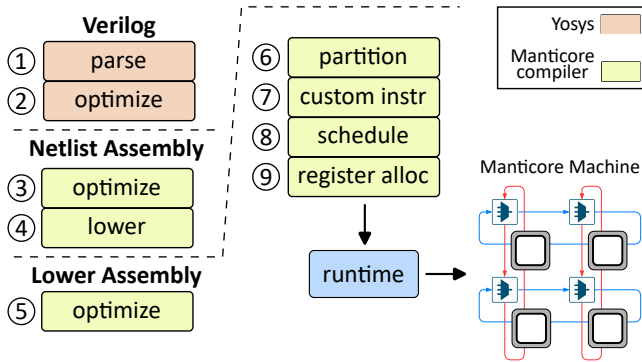


**Figure 6: Manticore compiler. Frontend in red, backend in green. A host communicates with the Manticore co-processor through a runtime shown in blue.**

instructions into an equivalent sequence of lower assembly instructions whose operands match Manticore’s 16-bit data path. Initially, the lower assembly is a monolithic sequence of instructions (a single process). After further optimizations, the compiler partitions the instructions into multiple processes. The compiler then optimizes each process by fusing chains of bitwise logic instructions into custom instructions.

The final steps of compilation are scheduling and register allocation. Scheduling ensures that there are no data hazards in the pipeline by inserting NOP instructions to respect data dependencies. In addition, the Send instructions must be scheduled to ensure timely message delivery. The compiler then maps virtual registers in the assembly program to machine registers and emits binary code. The binary is then loaded into Manticore over the NoC by a runtime running on a host x86. The Appendix contains more details about the runtime (§A.3).

The compiler is 18K lines of Scala. The Yosys Verilog frontend passes are about 2K lines of C++. The runtime is built on top of the Xilinx runtime library (XRT) with about 800 lines of C++ code.

## 6.1 Extracting Parallelism

Partitioning instructions across the cores is the most critical step in achieving good parallel performance. Despite the absence of runtime synchronization in Manticore, data movement is still costly and communication will limit scalability. Our parallelization algorithm is aware of this cost and attempts to reduce NoC traffic while distributing work across cores such that each core executes roughly the same number of instructions.

The compiler parallelizes a single monolithic assembly process in two steps: (1) *Split* the monolithic process into a maximal number of tiny processes. (2) *Merge* the split processes so that the total number of processes does not exceed the number of available cores.

Splitting closely follows the approach described in §3.2 and illustrated in Fig. 1. The compiler first creates a DAG representation of the monolithic process. It then uses a backward traversal to partition all nodes reachable from the sinks to form independent smaller processes. In creating the parallel processes, the compiler ensures that instructions that access the same memory region (e.g., an unpacked array in Verilog) end up in the same process to avoid moving large

amounts of data every Vcycle. Additionally, all privileged instructions must execute in the same process. Partitioning can duplicate DAG nodes across multiple cores, maximizing parallelism at the expense of increased computation.

If we view the maximal set of split processes as a graph whose nodes denote processes and edges denote communication, then merging is a hyper-graph partitioning problem. Existing partitioning tools [19, 34] assume a *linear* cost function, so merging two nodes adds their weight or cost. However, optimizations such as data sharing and duplicate code elimination make merging non-linear, so we instead developed a heuristic algorithm.

The compiler estimates the execution time of a process as the total number of instructions it executes, including Sends, but excluding the NOPs used to schedule data hazards and received messages. A vital goal of merging processes is to avoid overloaded cores (i.e., forming stragglers) by equalizing the execution time of all processes. The compiler iteratively picks two merge candidates that minimize the increase in merged execution time. It starts from the process with the shortest execution time and merges it with another process with which it communicates. This process is chosen to produce the smallest increase in execution time. Intuitively, by starting from the smallest processes and constructing larger ones, we can balance the execution time of the processes and simultaneously reduce communication (hence avoid network contention).

Merging can continue even after reaching the number of available cores because it can reduce execution time. For instance, merging processes p1 and p2 that read a value produced by process p3 could lower the execution time of p3 because it executes one fewer Send instruction. Furthermore, since splitting the DAGs may duplicate code, common sub-expression elimination in a merged process could reduce the number of instructions.

After the merge, the compiler assigns the process that contains privileged instructions to the privileged core. All other processes are mapped to cores using a random assignment. §7.6.2 evaluates other alternatives.

## 6.2 Custom Function Synthesis

Manticore’s instructions all have the same latency and programs are branch-free, so shorter programs are faster than longer ones. Custom function synthesis is the process of collapsing long chains of bitwise logic operations common in RTL simulation into a shallow sequence of 4-input custom functions. This process is conducted on each partitioned process independently. Instruction fusion borrows ideas from classical minimum-area, bit-level logic synthesis and applies them to word-level programs.

We start from a process’ dependence graph and prune all non-logic vertices. This leaves us with a set of connected components, each containing only logic operations. We exhaustively extract all 4-input *maximum fanout-free cones* (MFFC) from each component using cut enumeration [12]. An MFFC is a tree rooted at a terminal instruction such that no intermediate result is used by an instruction outside the cone. Multiple MFFCs can represent the same function and differ only in their representation. We use logic equivalence checking to group all MFFCs by the function they compute.

Finally we use a mixed-integer linear programming (MILP) formulation to maximize instruction savings by selecting the best set

of non-overlapping MFFCs, while considering that some MFFCs are used at multiple places and yield more savings. Each MFFC is then replaced with a single custom function. The MFFCs’ truth tables are used to configure each core’s CFU at boot time.

### 6.3 Scheduling, Routing, and Register Allocation

The compiler uses a simple list scheduling algorithm to schedule data hazards. It performs an abstract cycle-accurate simulation of one Vcycle with a model of a core’s pipeline and the NoC. An instruction is scheduled when its predecessors (in the DAG) are scheduled and executed. Additionally, a Send instruction can be issued only when it will not collide with any other messages on its path. If we cannot issue an instruction in a scheduling step, the compiler delays it with a NOP instruction.

A simple linear-scan register allocator works well with practically no spills because of the large register file.

Furthermore, we optimize redundant register moves by allocating the same machine register to both the current and next values of an RTL register (e.g., in Fig. 1, + and - values use the same machine register when possible) [41].

## 7 EVALUATION

### 7.1 Test Environment

We run Verilator 4.222 with an Intel Xeon E5-2680 v3 on Ubuntu 20.04. FPGA results are from the Alveo U200<sup>5</sup> datacenter FPGA using Vivado 2022.1 and XRT 2.13.466.

### 7.2 FPGA Prototype

We first evaluate the physical design of Manticore’s FPGA implementation. Table 1 reports the achieved frequency for various Manticore grids. The smaller grids can operate at *very* high speeds (close to 500MHz). There is abrupt degradation at the 12×12 grid, which is explainable by the FPGA’s physical layout. The U200’s rectangular floorplan is divided into (1) a static shell connected to the PCIe bus and (2) a user logic region. The vendor placed the shell at the center-right side of the chip, and it is immovable. User logic consequently has a C-shaped floorplan (Appendix §A.4 contains die-shots). With fewer than 160 cores, Manticore fits at the top of the chip, undisturbed by the shell. Additional cores spread around the shell, which makes timing closure difficult. We guide the place and route tool through floorplanning of designs with more than 160 cores. This significantly improves quality of results. Details are described in the Appendix (§A.4).

Grid	8×8	10×10	12×12	15×15	16×16
<b>Auto</b>	500	485	480	395	180
<b>Guided</b>	–	–	500	475	450

**Table 1: Achieved clock frequency (MHz) on U200 using automatic and guided floorplanning.**

<sup>5</sup>Static shell platform xilinx\_u200\_gen3x16\_xdma\_2\_202110\_1

Each core uses less than 0.021% of the U200’s resources. Available URAMs limit the number of cores to 398<sup>6</sup> [16] (Table 4 in the Appendix contains details).

### 7.3 Benchmarks

We evaluate Manticore’s performance with nine RTL workloads (we wrapped these benchmarks in simple, assertion-based Verilog test drivers):

- **bc** is a bitcoin miner [26].
- **mm** is a 16×16 integer matrix-matrix multiplier.
- **cgra** is a latency-insensitive, coarse-grained reconfigurable array of 64 floating-point processing elements.
- **vta** is a ML accelerator [22]. We use a larger<sup>7</sup> spatial implementation as the default configuration is too small to benefit from hardware acceleration. We divide buffer sizes by 4, so they fit in Manticore’s scratchpads.
- **rv32r** consists of 16 in-order pipelined RISC-V processors [20] communicating over a ring network.
- **jpeg** is a pipelined JPEG decoder [38].
- **blur** is a stencil computation accelerator [11].
- **mc** is a Monte-Carlo simulation stock option price evolution predictor with fixed-point arithmetic [36].
- **noc** is a 2D 4×4 uni-directional torus network-on-chip with wormhole routing and four virtual channels.

The state in all benchmarks is fully contained in on-chip scratchpads, so the compiler can accurately predict performance. We evaluate global stalls separately (§7.7).

### 7.4 End-to-End Performance

Fig. 7 compares Manticore and Verilator’s best performance normalized to Verilator’s single-thread performance. We disable waveform dumps and unnecessary printing to get undiluted performance metrics. Furthermore, we exclude initialization overhead to reflect *steady state* performance of long-running simulations. Initialization typically takes < 1s but requires multiple transitions between the host and the FPGA (see §A.3 for details).

Despite running at a fraction of the Xeon’s clock speed, Manticore outperforms single-thread Verilator, by a factor of up to 27.9×, for all workloads except jpeg. The low performance of jpeg results from two factors. First, jpeg is substantially smaller than other benchmarks (Table 3 in the Appendix) and does not contain enough parallelism. The compiler can improve its single-core performance by only ≈17% through parallelism as it contains unbalanced code paths. Second, there is a significant clock frequency and IPC difference between Manticore and Xeon. With only a handful of cores running at ≈500 MHz and a resulting *aggregate* IPC of 1.17, Manticore cannot compete with the Xeon’s ≈3.3 GHz multiple-issue pipeline that executes instructions at an average IPC of 2.25.

In summary, without sufficient parallelism, Manticore’s low-frequency processors cannot match the performance of a Xeon processor. On the other hand, the other measurements demonstrate that with enough parallelism, Manticore makes up for its lower single-thread performance and considerably outperforms Verilator. Moreover, Manticore does better with large designs as Verilator’s

<sup>6</sup>Out of 800 available URAMs, 4 are allocated to the cache.

<sup>7</sup>blockIn=64 and blockOut=64 instead of 16.

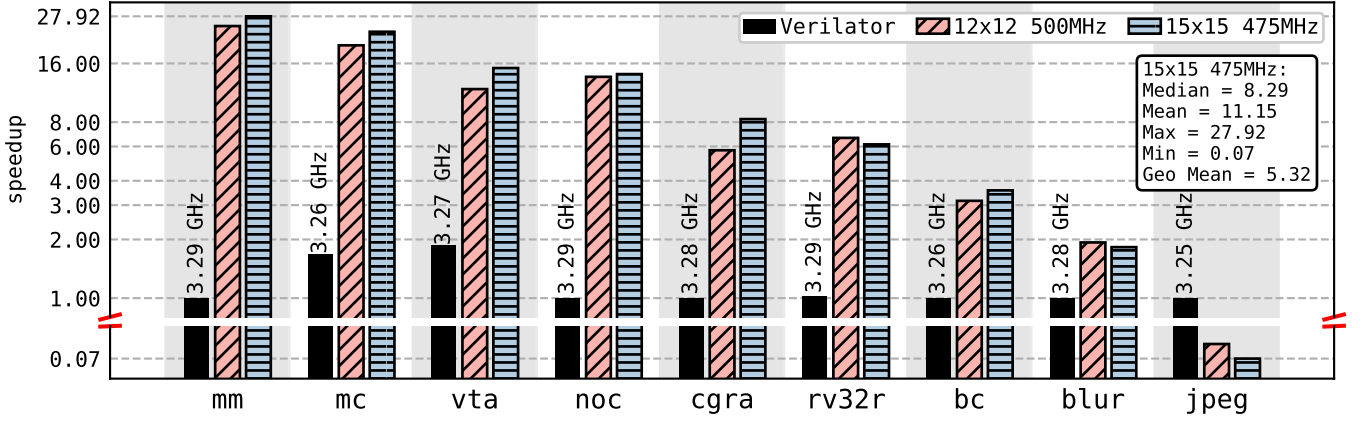


Figure 7: Manticore’s and Verilator’s speedup normalized against Verilator’s single-thread performance ( $\log_2$  scale). Verilator is multithreaded but achieves a speedup over its single-thread execution only for the *mc* and *vta* benchmarks. The numbers above the Verilator bars are the measured average CPU frequency during simulation. The peak speedup is  $27.9\times$  with a geometric mean speedup of  $5.3\times$  for a  $15\times 15$  grid.

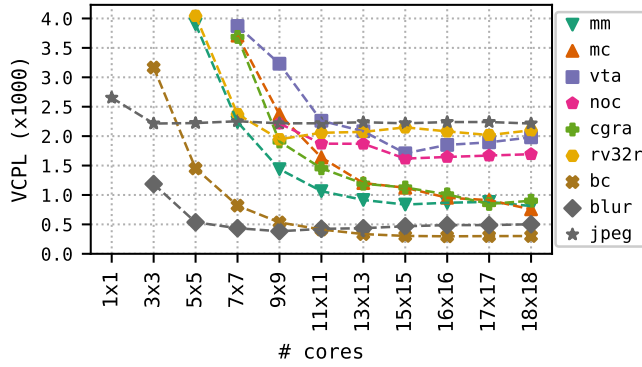


Figure 8: Manticore’s VCPL scaling (lower is better). Scaling past 225 cores yields diminishing returns.

IPC generally drops as design size increases, whereas Manticore’s aggregate IPC increases.

## 7.5 Scaling to 100s of Cores

With task-parallel workloads such as RTL, it is not immediately clear how performance might improve as the number of cores increases. Fig. 8 offers some insight. The virtual critical-path length (VCPL) is the total number of instructions (including NOPs) in the slowest core (i.e., the straggler). In the absence of dynamic behavior (off-chip DRAM accesses), the VCPL is proportional to execution time (or inverse of simulation rate).

Scaling stagnates at 225 ( $15\times 15$ ) cores for almost all benchmarks. Larger grids yield little benefit for the benchmarks. Increased performance might result from better compilation techniques or increased single-core performance (e.g., increasing clock speed with an ASIC implementation).

## 7.6 Compiler Techniques

The rest of the evaluation focuses on compilation techniques.

**7.6.1 Communication-Aware Partitioning.** The balanced partitioning algorithm (B) described in §6.1 merges the split processes while keeping communication costs low. As a baseline, we compare it against a communication-oblivious, longest processing-time first partitioning algorithm (L) to observe the benefits of modeling communication. Both algorithms are heuristic and use the same cost estimation method, but differ in their merge strategy. Furthermore, both algorithms are oblivious to the effects of instruction scheduling (which occurs after partitioning) as neither counts the NOPs inserted for data hazards and NoC contention.

Fig. 9 compares the two approaches for a  $15\times 15$  Manticore grid, with VPCL normalized to that of L. We subdivided the VCPL into the fraction of cycles spent on computing (compute), sending messages (send), or doing nothing (NOP) in the straggler. The numbers above each bar denote the number of cores used. Modeling communication is essential. B significantly reduces the total number of Sends (see Table 2), reduces the number of NOPs in the straggler, and generally outperforms (except for *vta*) the communication-oblivious algorithm (L) despite using fewer cores. As an example of the critical role of the partitioning algorithm, note that B reduces the VCPL by more than 50% in *bc*. Without B, the speedup in Fig. 7 would have been 60% instead of 325%.

$\times 1000$	mm	mc	vta	noc	cgra	rv32r	bc	blur	jpeg
<b>L</b>	23.3	23.6	13.6	25.6	18.9	16.9	7.7	5.0	1.0
<b>B</b>	8.5	3.9	9.8	16.6	7.4	2.8	3.1	2.7	0.1
%	-63.6	-83.5	-28.0	-35.3	-60.6	-83.3	-59.5	-47.1	-94.1

Table 2: Total Send instructions ( $\times 1000$ ) produced by *L* and *B*. *B* consistently reduces communication.



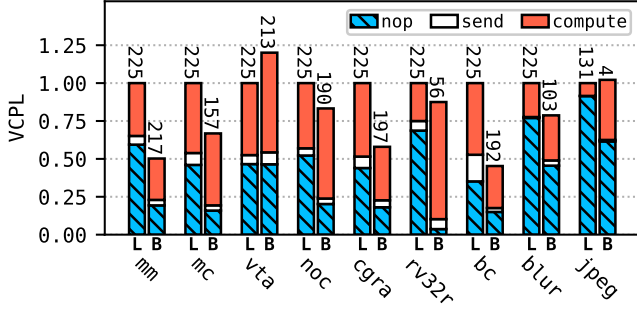


Figure 9: Comparison of the communication-oblivious, longest processing-time first algorithm (L) and the communication-aware algorithm from §6.1 (B) in the straggler on a 15x15 grid. VCPL is normalized to the VCPL of L. The numbers above each bar show the total number of cores used.

**7.6.2 Process-to-Core Placement.** Communication latency can be further reduced by assigning communicating processes to nearby cores on the torus NoC. We tried to find an optimal process-to-core assignment using a MILP formulation with objective functions such as minimizing the maximum or total link utilization. However, the problem became intractable with a grid size larger than 4x4, even with commercial solvers. Because of the uni-directional design of the torus, exchanging any two processes’ core assignments changes the cost of *all* communication links. This forces the solver to enumerate all 16! possible assignments for a 4x4 grid, which makes the solution intractable.

Alternatively, we used a tractable heuristic: recursively bi-partitioning the set of processes to minimize inter-partition communication. Counterintuitively, the bi-partitioning solutions were not systematically better than random placement. We analyzed this unexpected behavior and realized that most cores within the 90<sup>th</sup> percentile of the straggler’s Vcycle are compute-bound. Consequently, changes to process-to-core mapping could produce less than 10% performance improvement since they affect only communication-bound cores.

**7.6.3 Custom Instructions.** We initially formulated custom instructions to *cheaply* compensate for the lack of instruction-level parallelism (due to our single-issue pipeline) by exploiting bit-level parallelism seemingly abundant in RTL. Fig. 10 shows the VCPL of each benchmark normalized to the VCPL without custom instructions. The VCPL is broken down into custom instructions, Nops, and other types of instructions. The numbers above each bar show the reduction in total number of instructions over *all* cores (excluding Nops). This reduction is 2.9–17.8%, yet the VCPL (end-to-end) reduction is less than 10% in all benchmarks. Custom instructions reduce the *total* instruction count, but may not benefit the straggler (e.g., in jpeg). Eliminating the CFU from hardware would save one BRAM and a few tens of LUTs. However, this would not allow larger Manticore grids since the URAMs are the limiting resource.

**7.6.4 Compile Time.** The prototype compiler is built in Scala for robustness and compile times are in the order of minutes (max.

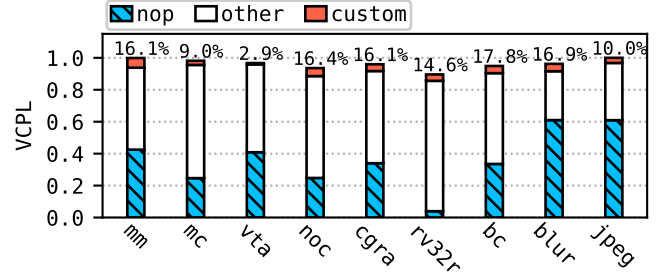


Figure 10: Savings in Vcycle due to custom instructions. The Vcycle is broken down into three instruction types and normalized to not using any custom functions. The numbers above each bar represent the reduction in non-Nop instructions over all cores.

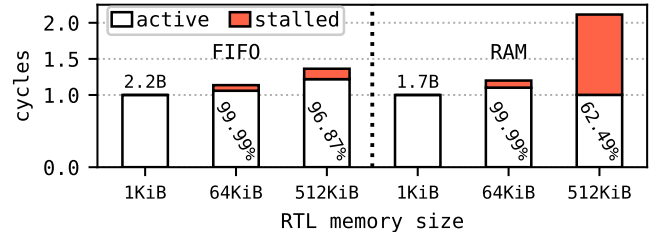


Figure 11: The total number of cycles (lower is better) spent simulating a FIFO (left) and a RAM (right). Numbers are normalized to the cycles needed to run the 1 KiB design. The numbers inside other bars denote the cache hit rate.

17m). This offers software development-like turnaround times for hours-long simulations. Most of the compilation time is spent in parallelization. A detailed discussion and breakdown is presented in §A.5.

## 7.7 Global Stall

We evaluate the impact of going off-chip with two RTL microbenchmarks running on a 1x1 Manticore grid at 500 MHz: (1) a FIFO, and (2) a RAM. The evaluated FIFO and RAM are 1 KiB, 64 KiB, and 512 KiB. The FIFO sequentially reads/writes its memory, whereas the RAM accesses its memory with pseudo-random addresses (using a simple XOR-shift-128 generator). Each program runs for 16Mi Vcycles performing one load and one store operation per Vcycle. We use hardware performance counters to log the total number of cycles, stalled cycles, cache hits, and cache misses. For each microbenchmark, the 1 KiB configuration serves as a baseline since this memory fits in the scratchpad, and there are no global stalls. The 64 KiB represents a middle point in which the state does not fit in the scratchpad but is fully contained within the 128 KiB cache. Lastly, the 512 KiB configuration corresponds to the scenario in which the state is spread between the on-chip cache and off-chip DRAM. Fig. 11 demonstrates that large FIFOs have a high hit rate and are not stall-limited (i.e., FIFOs have excellent cache locality). By contrast, large RAMs suffer as the number of off-chip accesses increases, which is the case in this experiment with completely

random accesses. Finally, we observe that cache accesses come at a cost even if they hit since we conservatively stall the execution on every such access.

## 8 LIMITATIONS AND FUTURE WORK

Our current prototype has  $\approx 7$  MiB of instruction memory (our FPGA is memory-limited), which may limit simulation capacity. ASICs can easily provision tens of MiBs of SRAM [37], greatly increasing simulation capacity. However, if a single device’s total on-chip memory cannot accommodate the working set, then the work must be partitioned across multiple Manticore grids (e.g., in a rack). Manticore’s reliance on static scheduling does not limit its implementation to a single FPGA, as it is possible to maintain determinism in a distributed system [1].

Manticore currently supports only one privileged core. This is an important limitation since all memories that do not fit in scratchpads are pinned to the privileged core, which can easily become a bottleneck. Our choice of a single privileged core was due to the ill-placed DRAM banks in our FPGA. A privileged core must be connected to a DRAM bank and cache, but the four DRAM banks in our FPGA are not adjacent. This makes floorplanning to achieve a high frequency very challenging and we decided to limit ourselves to Manticore’s single-bank performance for now. ASIC implementations would not have this floorplanning issue.

Manticore’s compiler currently supports only single-clock designs, but this is not a limitation of static BSP. In fact, multiple *synchronous* clocks can be simulated with static BSP as they have a *fixed* phase relation. Verilator can also handle such designs. In contrast, *asynchronous* clocks do not have a fixed phase relation and are out of the scope of full-cycle simulation<sup>8</sup>. Manticore’s strict static execution model disallows asynchronous clocks entirely.

Waveform debugging is an essential tool in a digital designer’s arsenal. It is possible to collect waveforms by using global stores, but this would result in excessive overhead. We have an initial design of hardware support for out-of-band waveform collection, but we leave its evaluation for future work.

## 9 RELATED WORK

### 9.1 FPGA Prototypes and Emulation Platforms

*FPGA prototypes* achieve interactive simulation speeds by mapping RTL circuits to *gates* on an FPGA. Prototypes can run full software stacks for trillions of clock cycles but require significant engineering effort and lack visibility. FireSim [18] is an open-source FPGA prototyping platform, widely used as an *architectural* simulator for exploring RISC-V designs at datacenter-scale using cloud FPGAs. *Emulation platforms* are RTL simulators for very large designs [30]. They provide excellent visibility into hardware state by mapping RTL circuits to *instructions* that run on a processor grid. Interconnecting multiple custom processor grids (in a rack) generally greatly increases simulation capacity. However, commercial emulation platforms cost millions of dollars [15].

Although Manticore is implemented on an FPGA, its simulation runs in software (a program running on Manticore) rather than being mapped to an FPGA. Consequently, Manticore’s compile

<sup>8</sup>[23] subverts Verilator’s static schedule with timestamped clocks to simulate multiple asynchronous clock domains.

times are a few minutes, whereas FPGA prototypes take hours to days to compile. Manticore is a first step towards an open-source alternative to commercial emulation platforms.

### 9.2 Parallel RTL simulation

There is considerable research on accelerating RTL simulation using parallelism, especially GPUs. Much of this work demonstrates significant speedups relative to commercial *event-driven* simulators. By contrast, Manticore is a *full-cycle* simulator, so it is not comparable to these systems. Most of this work focused on reducing the runtime overhead of monitoring value changes, for example, GCS [8–10] or Qian and Deng [29]. They improved simulation rates by orders of magnitude, to  $\approx 5$ –37 kHz, over single-threaded commercial simulators. Since Manticore is full-cycle, it immediately offers simulation rates above 150 kHz (see Fig. 8).

RTFlow [21] is a GPU-accelerated RTL simulator that exploits stimulus-level parallelism to speed up simulation by running many independent simulations on a GPU. RTFlow improves execution speed by up to 40 $\times$  over Verilator for many stimuli, but it runs an order magnitude slower than Verilator with a single stimulus. Manticore is faster than Verilator with a single stimulus.

Zhang [43] called for a renewal in GPU-accelerated RTL simulation research by leveraging recent advances in GPU-compute APIs designed for machine learning.

### 9.3 Sequential RTL Simulation

Most efforts in improving RTL simulation on CPUs focused on reducing the runtime overhead of event-driven simulation. ESSENT [4, 5] is a cycle-accurate simulator that employs a coarsened, conditional, singular, static (CCSS) execution model [4]. CCSS is a novel, hybrid approach that minimizes the overhead of runtime checks in event-driven simulation, especially in the presence of low activity factors. ESSENT is single-threaded and accelerates simulation of RISC-V cores (CPUs have low activity factors) by 1.5–11.5 $\times$  over Verilator. However, it is not clear how ESSENT performs with spatial designs that exhibit high activity factors, especially since it is single threaded [3]. Manticore’s performance is independent of a design’s activity factor.

Cuttlesim [27] is a cycle-accurate simulator for Kôika [6], a rule-based HDL derived from Bluespec Verilog [24]. Cuttlesim uses the high-level semantics of Kôika to generate C++ code optimized for sequential performance. It reports 2–3 $\times$  faster simulation than the equivalent RTL code running Verilator.

### 9.4 Deterministic Acceleration

Manticore’s design philosophy is similar to VLIW processors and other Raw machines [40]. A more recent example is Groq’s ML accelerator [1, 2]. The Groq chip has deterministic hardware datapaths that enable precise reasoning and control by software. Like RTL simulation, machine learning exhibits rare long-lived divergent code paths, which makes static scheduling feasible.

## 10 CONCLUSION

RTL simulation is essential for hardware design, and faster simulation offers many benefits to hardware designers. However, current approaches force a designer to choose between an FPGA prototype’s

long compile times and fast execution, or an RTL simulator's fast turnaround and slow speed. RTL simulation is slow because even state-of-the-art simulators struggle to exploit RTL circuits' abundant fine-grained parallelism to improve their performance due to the high cost of frequent communication and synchronization on modern processors.

This work presented Manticore, a prototype, hardware-accelerated RTL simulator. Manticore exposes a *deterministic* hardware interface that allows its compiler to *statically* schedule programs across hundreds of simple processors. This approach eliminates costly runtime synchronization and enables efficient parallel simulation of RTL circuits. Our FPGA prototype of Manticore demonstrated a peak speedup of  $27.9\times$  faster simulation rate (geomean  $5.3\times$ ) over a state-of-the-art software RTL simulator for Verilog workloads. This initial Manticore system demonstrates the performance benefits of exploiting fine-grained parallelism in RTL code.

## REFERENCES

- [1] Dennis Abts, Garrin Kimmell, Andrew C. Ling, John Kim, Matthew Boyd, Andrew Bitar, Sahil Parmar, Ibrahim Ahmed, Roberto DiCecco, David Han, John Thompson, Michael Bye, Jennifer Hwang, Jeremy Fowers, Peter Lillian, Ashwin Murthy, Elyas Mehtabuddin, Chetan Tekur, Thomas Sohmers, Kris Kang, Stephen Maresh, and Jonathan Ross. 2022. A software-defined tensor streaming multiprocessor for large-scale machine learning. In *ISCA '22: The 49th Annual International Symposium on Computer Architecture, New York, New York, USA, June 18 - 22, 2022*, Valentina Salapura, Mohamed Zahran, Fred Chong, and Lingjia Tang (Eds.). ACM, 567–580. <https://doi.org/10.1145/3470496.3527405>
- [2] Dennis Abts, Jonathan Ross, Jonathan Sparling, Mark Wong-VanHaren, Max Baker, Tom Hawkins, Andrew Bell, John Thompson, Temesghen Kahsai, Garrin Kimmell, Jennifer Hwang, Rebekah Leslie-Hurd, Michael Bye, E. R. Creswick, Matthew Boyd, Mahitha Venigalla, Evan Lafore, Jon Purdy, Purushotham Kamath, Dinesh Maheshwari, Michael Beidler, Geert Rosseel, Omar Ahmad, Gleb Gagarin, Richard Czekalski, Ashay Rane, Sahil Parmar, Jeff Werner, Jim Sproch, Adrian Macias, and Brian Kurtz. 2020. Think Fast: A Tensor Streaming Processor (TSP) for Accelerating Deep Learning Workloads. In *47th ACM/IEEE Annual International Symposium on Computer Architecture, ISCA 2020, Valencia, Spain, May 30 - June 3, 2020*. IEEE, 145–158. <https://doi.org/10.1109/ISCA45697.2020.00023>
- [3] Scott Beamer. 2020. A Case for Accelerating Software RTL Simulation. *IEEE Micro* 40, 4 (2020), 112–119. <https://doi.org/10.1109/MM.2020.2997639>
- [4] Scott Beamer and David Donofrio. 2020. Efficiently Exploiting Low Activity Factors to Accelerate RTL Simulation. In *57th ACM/IEEE Design Automation Conference, DAC 2020, San Francisco, CA, USA, July 20-24, 2020*. IEEE, 1–6. <https://doi.org/10.1109/DAC18072.2020.9218632>
- [5] Scott Beamer, Thomas Nijssen, Krishna Pandian, and Kyle Zhang. 2021. ESSENT: A high-performance RTL simulator. In *Workshop on Open-Source EDA Technology (WOSET), at International Conference on Computer-Aided Design (ICCAD)*.
- [6] Thomas Bourgeat, Clément Pit-Claudel, Adam Chlipala, and Arvind. 2020. The essence of Bluespec: a core language for rule-based hardware design. In *Proceedings of the 41st ACM SIGPLAN International Conference on Programming Language Design and Implementation, PLDI 2020, London, UK, June 15-20, 2020*, Alastair F. Donaldson and Emina Torlak (Eds.). ACM, 243–257. <https://doi.org/10.1145/3385412.3385965>
- [7] Adrian M. Caulfield, Eric S. Chung, Andrew Putnam, Hari Angepat, Jeremy Fowers, Michael Haselman, Stephen Heil, Matt Humphrey, Puneet Kaur, Joo-Young Kim, Daniel Lo, Todd Massengill, Kalin Ovtcharov, Michael Papamichael, Lisa Woods, Sitaram Lanka, Derek Chiou, and Doug Burger. 2016. A cloud-scale acceleration architecture. In *49th Annual IEEE/ACM International Symposium on Microarchitecture, MICRO 2016, Taipei, Taiwan, October 15-19, 2016*. IEEE Computer Society, 7:1–7:13. <https://doi.org/10.1109/MICRO.2016.7783710>
- [8] Debapriya Chatterjee, Andrew DeOrio, and Valeria Bertacco. 2009. Event-driven gate-level simulation with GP-GPUs. In *Proceedings of the 46th Design Automation Conference, DAC 2009, San Francisco, CA, USA, July 26-31, 2009*. ACM, 557–562. <https://doi.org/10.1145/1629911.1630056>
- [9] Debapriya Chatterjee, Andrew DeOrio, and Valeria Bertacco. 2009. GCS: High-performance gate-level simulation with GPGPUs. In *Design, Automation and Test in Europe, DATE 2009, Nice, France, April 20-24, 2009*, Luca Benini, Giovanni De Micheli, Bashir M. Al-Hashimi, and Wolfgang Müller (Eds.). IEEE, 1332–1337. <https://doi.org/10.1109/DATE.2009.5090871>
- [10] Debapriya Chatterjee, Andrew DeOrio, and Valeria Bertacco. 2011. Gate-Level Simulation with GPU Computing. *ACM Trans. Design Autom. Electr. Syst.* 16, 3 (2011), 30:1–30:26. <https://doi.org/10.1145/1970353.1970363>
- [11] Jason Cong, Peng Li, Bingjun Xiao, and Peng Zhang. 2014. An Optimal Microarchitecture for Stencil Computation Acceleration Based on Non-Uniform Partitioning of Data Reuse Buffers. In *The 51st Annual Design Automation Conference 2014, DAC '14, San Francisco, CA, USA, June 1-5, 2014*. ACM, 77:1–77:6. <https://doi.org/10.1145/2593069.2593090>
- [12] Jason Cong, Chang Wu, and Yuzheng Ding. 1999. Cut Ranking and Pruning: Enabling a General and Efficient FPGA Mapping Solution. In *Proceedings of the 1999 ACM/SIGDA Seventh International Symposium on Field Programmable Gate Arrays, FPGA 1999, Monterey, CA, USA, February 21-23, 1999*, Sinan Kaptanoglu and Steve Trimberger (Eds.). ACM, 29–35. <https://doi.org/10.1145/296399.296425>
- [13] Peter Flake, Phil Moorby, Steve Golsen, Arturo Salz, and Simon J. Davidmann. 2020. Verilog HDL and its ancestors and descendants. *Proc. ACM Program. Lang.* 4, HOPL (2020), 87:1–87:90. <https://doi.org/10.1145/3386337>
- [14] John L. Hennessy and David A. Patterson. 2019. A new golden age for computer architecture. *Commun. ACM* 62, 2 (2019), 48–60. <https://doi.org/10.1145/3282307>
- [15] Jim Hogan. 2018. Hogan compares Palladium, Veloce, EVE ZeBu, Aldec, Bluespec, Dini. online.
- [16] Xilinx Inc. 2022. *Alveo data center accelerator card platforms*. Xilinx Inc. <https://docs.xilinx.com/r/en-US/ug1120-alveo-platforms/U200-Gen3x16-XDMA-base-2-Platform>
- [17] Nachiket Kapre and Jan Gray. 2017. Hoplite: A Deflection-Routed Directional Torus NoC for FPGAs. *ACM Trans. Reconfigurable Technol. Syst.* 10, 2 (2017), 14:1–14:24. <https://doi.org/10.1145/3027486>
- [18] Sagar Karandikar, Howard Mao, Donggyu Kim, David Biancolin, Alon Amid, Dayeol Lee, Nathan Pemberton, Emmanuel Amaro, Colin Schmidt, Aditya Chopra, Qijing Huang, Kyle Kovacs, Borivoje Nikolic, Randy H. Katz, Jonathan Bachrach, and Krste Asanovic. 2018. FireSim: FPGA-Accelerated Cycle-Exact Scale-Out System Simulation in the Public Cloud. In *45th ACM/IEEE Annual International Symposium on Computer Architecture, ISCA 2018, Los Angeles, CA, USA, June 1-6, 2018*, Murali Annavaram, Timothy Mark Pinkston, and Babak Falsafi (Eds.). IEEE Computer Society, 29–42. <https://doi.org/10.1109/ISCA.2018.00014>
- [19] George Karypis, Rajat Aggarwal, Vipin Kumar, and Shashi Shekhar. 1999. Multilevel hypergraph partitioning: applications in VLSI domain. *IEEE Trans. Very Large Scale Integr. Syst.* 7, 1 (1999), 69–79. <https://doi.org/10.1109/92.748202>
- [20] Donggyu Kim. [n.d.]. riscv-mini. <https://github.com/ucb-bar/riscv-mini>
- [21] Dian-Lun Lin, Haoxing Ren, Yanqing Zhang, and Tsung-Wei Huang. 2022. From RTL to CUDA: A GPU Acceleration Flow for RTL Simulation with Batch Stimulus. In *International Conference on Parallel Processing (ICPP)*.
- [22] Thierry Moreau, Tianqi Chen, Luis Vega, Jared Roesch, Eddie Q. Yan, Lianmin Zheng, Josh Fromm, Ziheng Jiang, Luis Ceze, Carlos Guestrin, and Arvind Krishnamurthy. 2019. A Hardware-Software Blueprint for Flexible Deep Learning Specialization. *IEEE Micro* 39, 5 (2019), 8–16. <https://doi.org/10.1109/MM.2019.2928962>
- [23] Handling multiple clock with Verilator. [n.d.]. <http://zipcpu.com/blog/2018/09/06/tbclock.html>
- [24] Rishiyur S. Nikhil. 2004. Bluespec System Verilog: efficient, correct RTL from high level specifications. In *2nd ACM & IEEE International Conference on Formal Methods and Models for Co-Design (MEMOCODE 2004), 23-25 June 2004, San Diego, California, USA, Proceedings*. IEEE Computer Society, 69–70. <https://doi.org/10.1109/MEMOCOD.2004.1459818>
- [25] Thomas Norrie, Nishant Patil, Doe Hyun Yoon, George Kurian, Sheng Li, James Laudon, Cliff Young, Norman P. Jouppi, and David A. Patterson. 2021. The Design Process for Google's Training Chips: TPUv2 and TPUv3. *IEEE Micro* 41, 2 (2021), 56–63. <https://doi.org/10.1109/MM.2021.3058217>
- [26] Open-Source FPGA Bitcoin Miner. [n.d.]. <https://github.com/proganism/Open-Source-FPGA-Bitcoin-Miner>
- [27] Clément Pit-Claudel, Thomas Bourgeat, Stella Lau, Arvind, and Adam Chlipala. 2021. Effective simulation and debugging for a high-level hardware language using software compilers. In *ASPLOS '21: 26th ACM International Conference on Architectural Support for Programming Languages and Operating Systems, Virtual Event, USA, April 19-23, 2021*, Tim Sherwood, Emery D. Berger, and Christos Kozyrakis (Eds.). ACM, 789–803. <https://doi.org/10.1145/3445814.3446720>
- [28] Andrew Putnam, Adrian M. Caulfield, Eric S. Chung, Derek Chiou, Kypros Constantinides, John Demme, Hadi Esmaeilzadeh, Jeremy Fowers, Gopi Prashanth Gopal, Jan Gray, Michael Haselman, Scott Hauck, Stephen Heil, Amir Hormati, Joo-Young Kim, Sitaram Lanka, James R. Larus, Eric Peterson, Simon Pope, Aaron Smith, Jason Thong, Phillip Yi Xiao, and Doug Burger. 2014. A reconfigurable fabric for accelerating large-scale datacenter services. In *ACM/IEEE 41st International Symposium on Computer Architecture, ISCA 2014, Minneapolis, MN, USA, June 14-18, 2014*. IEEE Computer Society, 13–24. <https://doi.org/10.1109/ISCA.2014.6853195>
- [29] Hao Qian and Yangdong Deng. 2011. Accelerating RTL simulation with GPUs. In *2011 IEEE/ACM International Conference on Computer-Aided Design, ICCAD 2011, San Jose, California, USA, November 7-10, 2011*, Joel R. Phillips, Alan J. Hu, and Helmut Graeb (Eds.). IEEE Computer Society, 687–693. <https://doi.org/10.1109/ICCAD.2011.6105404>
- [30] Lauro Rizzatti and Charley Selvidge. 2020. Designing a Modern Hardware Emulation Platform. online.

- [31] Kamil Rocki, Dirk Van Essendelft, Ilya Sharapov, Robert Schreiber, Michael Morrison, Vladimir Kibardin, Andrey Portnoy, Jean-Francois Dietiker, Madhava Syamal, and Michael James. 2020. Fast stencil-code computation on a wafer-scale processor. In *Proceedings of the International Conference for High Performance Computing, Networking, Storage and Analysis, SC 2020, Virtual Event / Atlanta, Georgia, USA, November 9-19, 2020*, Christine Cuicchi, Irene Qualters, and William T. Kramer (Eds.). IEEE/ACM, 58. <https://doi.org/10.1109/SC41405.2020.00062>
- [32] Vivek Sarkar and John L. Hennessy. 1986. Compile-time partitioning and scheduling of parallel programs. In *Proceedings of the 1986 SIGPLAN Symposium on Compiler Construction, Palo Alto, California, USA, June 25-27, 1986*, Richard L. Wexelblat (Ed.). ACM, 17–26. <https://doi.org/10.1145/12276.13313>
- [33] Kaz Sato and Clif Young. 2017. An in-depth look at Google's first Tensor Processing Unit (TPU).
- [34] Sebastian Schlag, Tobias Heuer, Lars Gottesbüren, Yaroslav Akhremtsev, Christian Schulz, and Peter Sanders. 2021. High-Quality Hypergraph Partitioning. *CoRR* abs/2106.08696 (2021). arXiv:2106.08696 <https://arxiv.org/abs/2106.08696>
- [35] Wilson Snyder. [n.d.]. Verilator, Accelerated: Accelerating development, and case study of accelerating performance. ([n.d.]). [https://veripool.org/papers/Verilator\\_Accelerated\\_OSDA2020.pdf](https://veripool.org/papers/Verilator_Accelerated_OSDA2020.pdf) 2nd Workshop on Open-Source Design Automation (OSDA).
- [36] Xiang Tian and Khaled Benkrid. 2008. Design and implementation of a high performance financial Monte-Carlo simulation engine on an FPGA supercomputer. In *2008 International Conference on Field-Programmable Technology, FPT 2008, Taipei, Taiwan, December 7-10, 2008*, Tarek A. El-Ghazawi, Yao-Wen Chang, Juinn-Dar Huang, and Proshanta Saha (Eds.). IEEE, 81–88. <https://doi.org/10.1109/FPT.2008.4762369>
- [37] Yatish Turakhia, Gill Bejerano, and William J. Dally. 2018. Darwin: A Genomics Co-processor Provides up to 15, 000X Acceleration on Long Read Assembly. In *Proceedings of the Twenty-Third International Conference on Architectural Support for Programming Languages and Operating Systems, ASPLOS 2018, Williamsburg, VA, USA, March 24-28, 2018*, Xipeng Shen, James Tuck, Ricardo Bianchini, and Vivek Sarkar (Eds.). ACM, 199–213. <https://doi.org/10.1145/3173162.3173193>
- [38] ultraembedded. [n.d.]. High throughput JPEG decoder. [https://github.com/ultraembedded/core\\_jpeg](https://github.com/ultraembedded/core_jpeg).
- [39] Leslie G. Valiant. 1990. A Bridging Model for Parallel Computation. *Commun. ACM* 33, 8 (1990), 103–111. <https://doi.org/10.1145/79173.79181>
- [40] Elliot Waingold, Michael B. Taylor, Devabhaktuni Srikrishna, Vivek Sarkar, Walter Lee, Victor Lee, Jang Kim, Matthew I. Frank, Peter Finch, Rajeev Barua, Jonathan Babb, Saman P. Amarasinghe, and Anant Agarwal. 1997. Baring It All to Software: Raw Machines. *Computer* 30, 9 (1997), 86–93. <https://doi.org/10.1109/2.612254>
- [41] Christian Wimmer and Michael Franz. 2010. Linear scan register allocation on SSA form. In *Proceedings of the CGO 2010, The 8th International Symposium on Code Generation and Optimization, Toronto, Ontario, Canada, April 24-28, 2010*, Andreas Moshovos, J. Gregory Steffan, Kim M. Hazelwood, and David R. Kaeli (Eds.). ACM, 170–179. <https://doi.org/10.1145/1772954.1772979>
- [42] Claire Wolf. [n.d.]. Yosys Open SYnthesis Suite. <https://yosyshq.net/yosys/>.
- [43] Yanqing Zhang, Haoxing Ren, and Bruce Khailany. 2020. Opportunities for RTL and Gate Level Simulation using GPUs (Invited Talk). In *IEEE/ACM International Conference On Computer Aided Design, ICCAD 2020, San Diego, CA, USA, November 2-5, 2020*. IEEE, 166:1–166:5. <https://doi.org/10.1145/3400302.3415773>

## A APPENDIX

This appendix contains supplementary material that elaborates on points raised in the body of this paper.

### A.1 Verilator’s Performance

We profiled nine benchmarks with Intel’s VTune profiler to study Verilator’s performance. We measured the fraction of empty CPU pipeline slots (bubbles) caused by three types of events:

- **front-end** bubbles caused by instruction cache misses,
- **core** bubbles due to software dependencies (i.e., data hazard) or insufficient functional units, and
- **memory** bubbles caused by cache misses.

Fig. 13 shows these metrics for each benchmark. The height of a plot shows the CPU’s underutilized pipeline slots on the left axis (lower is better). The dark line shows the dynamic instruction count normalized to single-thread execution on the right axis (lower is better). In all benchmarks, as the parallelism increases, the simulation becomes memory-bound and experiences a sharp increase in instruction count.

### A.2 Microarchitecture

Fig. 14 outlines the pipelined implementation of one core. The pipeline is 14 stages deep and is logically divided into the typical five functions: fetch, decode, execute, memory access, and writeback. The CFU is implemented as 16 LUTRAMs.

The pipeline’s frontend (right side of Fig. 14) is responsible for receiving messages during simulation. Each message is translated on the fly to a SET instruction and is written into instruction memory. A SET instruction updates a register with an immediate value. A state machine controls the execution of the pipeline, which is kept in strict lock-step with all other cores. The compiler inserts sleep instructions to coordinate communication between cores. An additional state machine handles incoming messages from the bootloader (see §A.3.1) and fills the instruction memory before the simulation starts.

### A.3 Runtime

Manticore’s runtime is a program running on the host processor that takes a binary generated by the compiler and runs it on the Manticore hardware accelerator connected to the host. The runtime copies the program binary into FPGA DRAM, then instructs the hardware bootloader (see Fig. 5) to copy the program into the local instruction memories. While the code executes, the runtime continuously polls the hardware state registers to handle exceptions or terminate execution.

**A.3.1 Bootloader.** Bootloading starts with a soft reset that brings all cores to a *boot state*. The soft reset only changes a few state registers in each core; it does not reset the register files or the scratchpads.

Cores continuously push NOPs through their pipelines and snoop the NoC for instructions when in the boot state. A hardware bootloader (see Fig. 5) module reads the program binary from DRAM and streams the instructions to each core in sequence. Cores store the incoming instructions in their instruction memory. The cores then wait for a message from the NoC that contains a core-specific

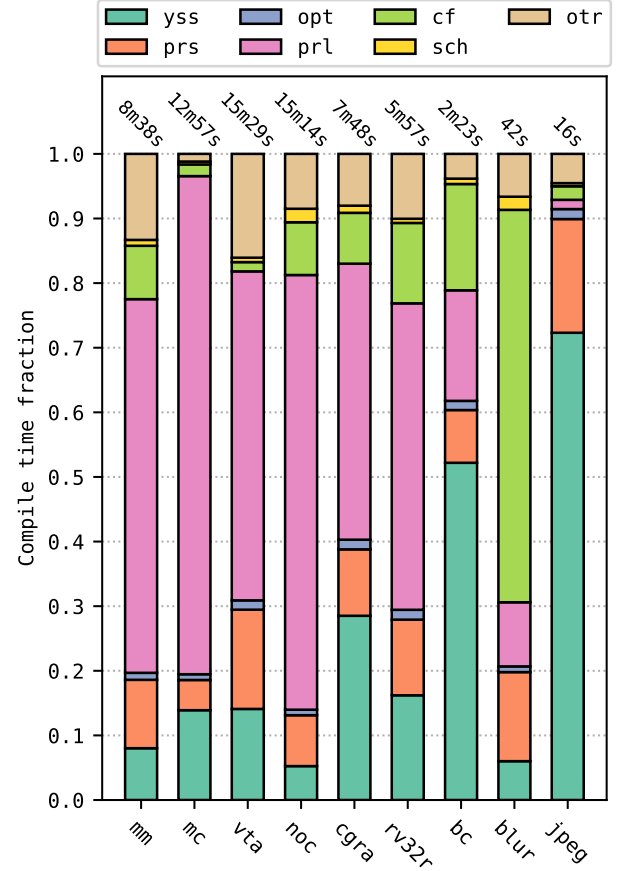


**Figure 12: Breakdown of compilation time: Yosys (yss), assembly parsing (prs), basic optimizations (opt), parallelization (prl), custom function extraction (cf), scheduling (sch), others (otr).**

countdown value. At that point, the cores initialize a local timer with their specific countdown and start execution when the timer counts down to 0. The countdown starts all cores simultaneously despite the non-deterministic time required to read a program binary from DRAM.

Fig. 14 shows the instruction stream format that a core receives. This stream consists of a header that encodes the number of instructions in a program and a footer comprised of three words:

- (1) EPILOGUE\_LENGTH denotes the total number of messages the core expects to receive at every Vcycle.
- (2) SLEEP\_LENGTH denotes the sleep period length (see sleep in Fig. 4).
- (3) COUNT\_DOWN is the last word received that initiates a countdown to the start.

**A.3.2 Exceptions.** Manticore’s hardware design and execution model make it possible to pause the execution, perform some computation on the host, and resume the execution on the FPGA. An example can illustrate this. Consider the following Verilog statement:



Bench	E	V	# instr	LoC	Compile Time		
					Manticore	Verilator	Verilator -j24
jpeg	1005	131	2905	6542	17s	7s	3s
blur	9649	751	5975	3869	59s	22s	15s
bc	8135	4630	21699	276	2m26s	40s	27s
mm	89102	6659	56568	64963	9m42s	7m5s	2m55s
rv32r	60430	4497	65488	31761	6m41s	1m56s	29s
noc	114364	6927	80718	39363	17m39s	3m23s	36s
cgra	57532	4615	82682	104498	8m36s	2m15s	37s
mc	52330	9182	102295	30353	13m34s	1m13s	16s
vta	56142	7037	114474	190818	15m44s	2m33	26s

**Table 3: Manticore, single-thread compile Verilator and 24-thread compile Verilator (-j24) compilation times.** |E| and |V| respectively denote the number of edges and nodes in the graph obtained by splitting each benchmark into a maximal set of independent processes (see §6.1). # instr denotes the number of lower assembly instructions before splitting in the single monolithic process. LoC denotes the Verilog/SystemVerilog lines of code for each benchmark. The benchmarks are sorted by # instr.

	LUT	LUTRAM	FF	BRAM	URAM	DSP	SRL
#	545	128	1358	4	2	1	102
%	0.05	0.02	0.05	0.19	0.21	0.01	0.02

**Table 4: Resource utilization of a single core on the U200. Percentages are the fraction of the total resources available on an U200.**

```
if (count != 0) $display("got %d", count);
```

This statement is executed as a global store instruction predicated by the condition `count != 0` that stores `count` to the global memory. The `$display` system call is translated to an `EXPECT` instruction that throws an exception when `count` is non-zero. When Manticore raises the exception, the grid stalls globally, and the host flushes the cache and reads the value of `count` from the FPGA DDR memory. The runtime prints this value for the user. Currently, our compiler only supports basic Verilog system calls. We plan to support arbitrary DPI (Verilog Direct Programming Interface) calls through this mechanism. However, crossing the host-device boundary is very expensive and should be avoided as much as possible.

## A.4 Floorplanning

The U200 is a large *multi-die* FPGA that contains three SLRs<sup>9</sup>. Inter-SLR connections are significantly more costly than intra-SLR ones. While Vivado can find an efficient floorplan of Manticore’s torus structure when the full design fits in a single SLR, it fails to do so when SLR crossings are necessary (see Fig. 15).

We get around this limitation by using a floorplanning script to guide Vivado. Cores do not directly access the shell and communicate only with their corresponding switch through a pipelined path. Therefore, cores do not need to respect a torus topology, so we spread half the cores in the top SLR and the other half in the bottom SLR. However, the NoC switches must be connected in a torus structure, so we constrain them to the narrow rectangular region in the central SLR. We constrain Vivado to use a set of dedicated hard registers available for crossing SLRs for each core-to-switch connection. We also co-locate the privileged core, cache, bootloader, and clock control logic in the central SLR as they access the shell. Finally, we minimize clock skew between the compute and control clock domains by assigning the clock buffers and clock roots to the same clock region. These optimizations enable a 15×15 grid to run at 475 MHz.

## A.5 Compile Time Analysis

Table 3 reports the compilation times of each benchmark for both Manticore and Verilator (single-thread and multi-thread). Manticore’s compiler is written in Scala and runs on the JVM, whereas Verilator is written in C++. Fig. 12 contains a detailed breakdown of compilation steps and their contribution to the total time. Most of the compile-time is spent in parallelizing RTL code. We expect to improve compilation time (it is currently unoptimized).

## A.6 FPGA resource utilization

Table 4 reports FPGA resource utilization for a single core. The dominant resource is the URAM, as two are required per core (one for the instruction memory and one for the local scratchpad). This limits the total number of cores on the U200 to 398. However, as discussed in the evaluation, a 225-element grid is usually the breaking point in scaling (see Fig. 8). As all cores may not use their scratchpad memory, one optimization is a heterogeneous implementation where some cores lack a scratchpad and rely on only a large register file so that other cores can have more local memory. We leave heterogeneous processor grids to future work.

<sup>9</sup>Super Logic Regions, Xilinx terminology for a single die.

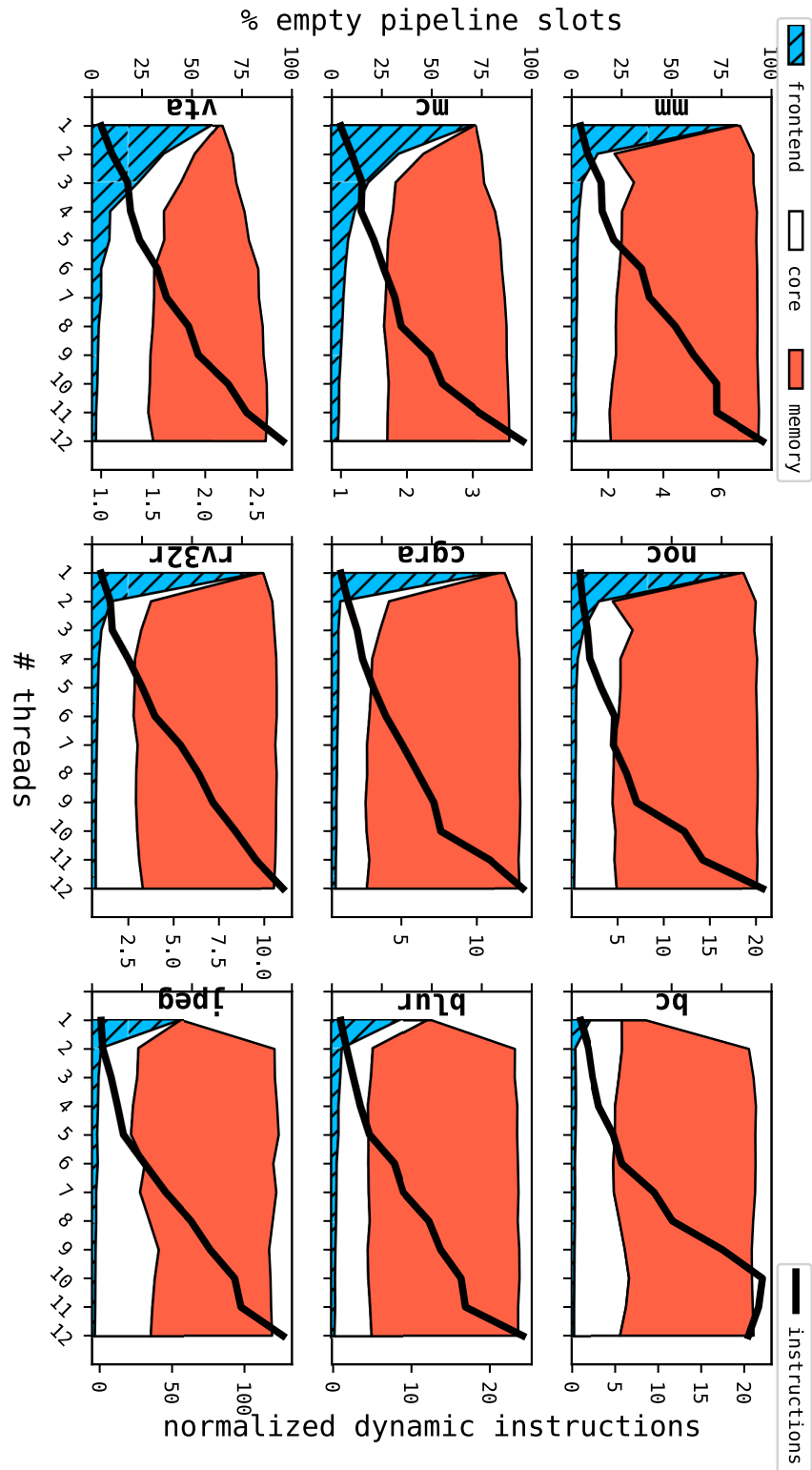


Figure 13: Verilator performance on an Intel Xeon E5-2680 v3. Breakdown of CPU empty pipeline slots on the left axis and executed instruction (normalized to single-thread) on the right axis.

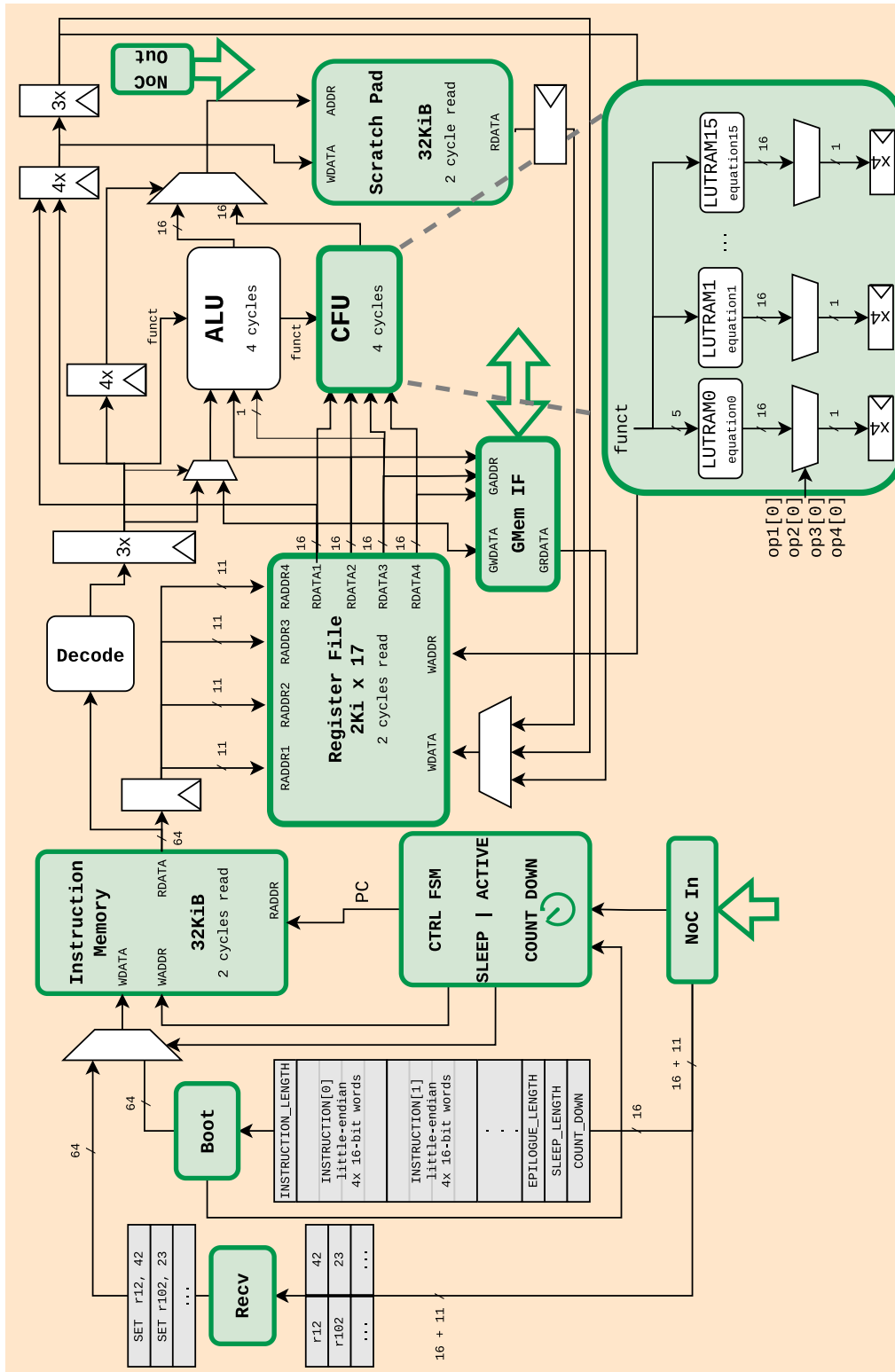


Figure 14: Microarchitecture of a core in Manticore's processor grid. Details are omitted for legibility.

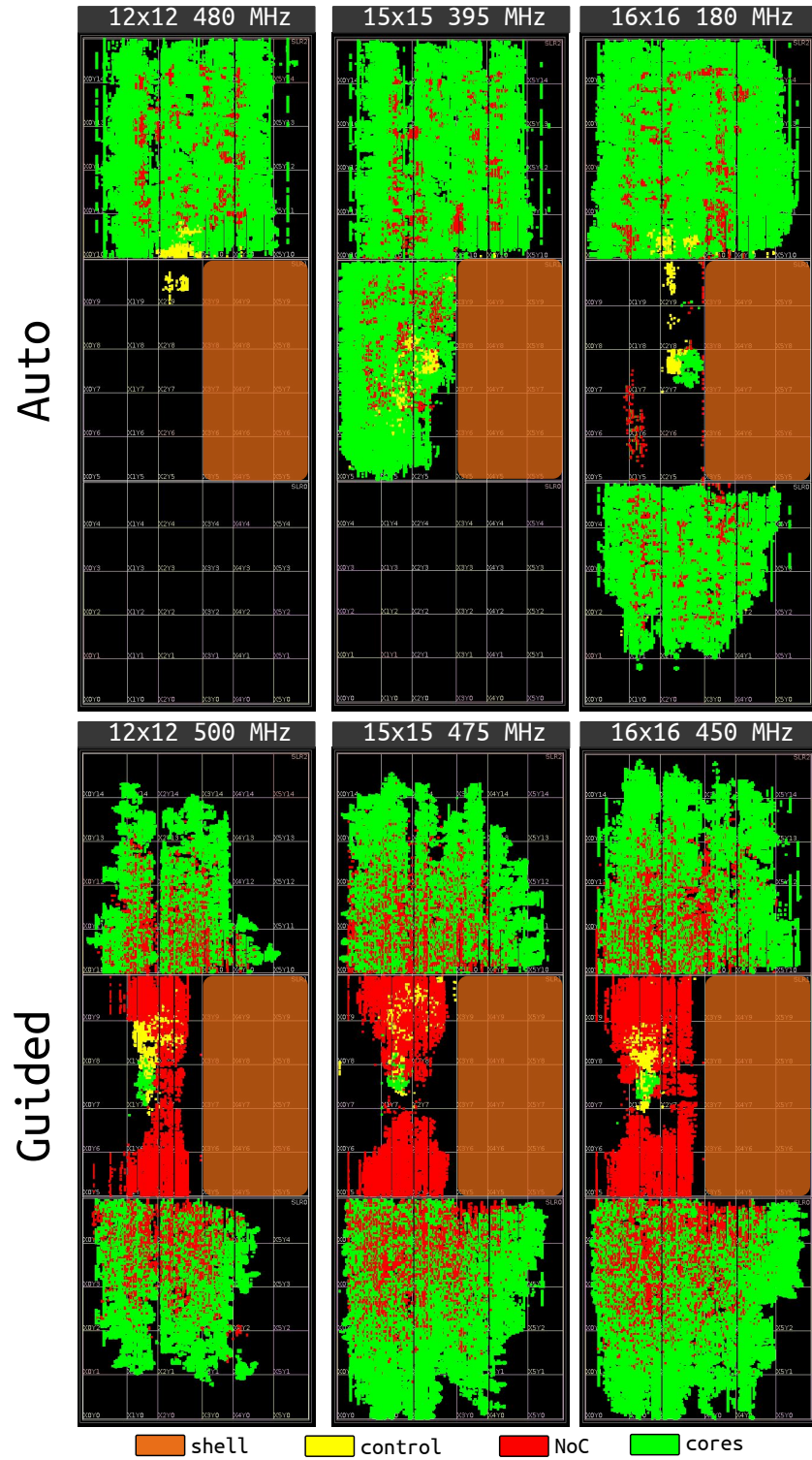


Figure 15: Floorplan of Manticore’s physical implementation on U200. Vivado’s automatic floorplanning is at the top and our guided floorplanning is at the bottom. The cores are colored in green, the NoC in red, and the control clock domain in yellow. The fixed shell is marked as an orange box in each floorplan. The clock speed is considerably higher with the guided floorplans.